The Dehydrogenation of Butane on Metal-Free Graphene

Alastair Brooks, Stephen J. Jenkins

Department of Chemistry, University of Cambridge, Lensfield Road, Cambridge, CB2 1EW, UK

Sabine Wrabetz

Fritz-Haber-Institut der Max-Planck-Gesellschaft, Abteilung Anorganische Chemie, c/o IRIS Adlershof, Zum Großen Windkanal 2, 12489 Berlin, Germany

James McGregor

Department of Chemical & Biological Engineering, University of Sheffield,Mappin Street, Sheffield, S1 3JD

*Marco Sacchi**

Department of Chemistry, University of Surrey, Guildford, GU2 7XH, UK

*email: m.sacchi@surrey.ac.uk

RECEIVED DATE

Abstract

The dehydrogenation of alkane feedstock to produce alkenes is a significant and energy intensive industrial process, generally occurring on metals and metal oxides. Here, we investigate a catalytic mechanism for the dehydrogenation of butane on single-layer, metal-free graphene using a combination of *ab initio* quantum chemical calculations and Adsorption Microcalorimetry. Dispersion-corrected Density Functional Theory (DFT) is employed to calculate transition states and energy minima that describe the reaction pathways connecting butane to the two possible products, but-1-ene and but-2-ene. The deprotonations occur with moderate energy barriers in the 0.54 eV ÷ 0.69 eV range. A strong agreement is observed between the results of the adsorption energies calculated by DFT (0.40 eV) and the measured differential heat of adsorption of n-butane on graphitic overlayer. We conclude that the active-site for this catalytic reaction is a metal-free graphene vacancy, created by removing a carbon atom from a single-layer graphene sheet.

Keywords: graphene catalysis, dehydrogenation, metal-free catalysis, graphene vacancy, density functional theory

1. Introduction

Much hope has been placed in graphene, both for its enormous potential in disruptive technological applications and for its current role as a playground material for studying quantum phenomena. The creation of graphene in the laboratory[1], in 2004, has opened up an exciting perspective as ideal 2D flat surfaces, formerly encountered only in theoretical models, became suddenly available for a wide range of experiments and applications. More recently, flakes of graphene have been created on a macroscopic scale, up to one mm, and are visible to the naked eye.[2] Electronic excitations in the graphene sheet have unusual dispersion properties and behave as massless fermions described by a Dirac equation,[2] displaying both relativistic and quantum features, and providing an unrivalled opportunity to validate unusual theoretical predictions, for example Klein tunnelling. [3-4]

Graphene also exhibits a long list of record-breaking properties, for instance high thermal and electrical conductivity and high Young's modulus.[2, 5-6] Although most of the experimental and theoretical work on graphene has been focussed on its electronic and physical properties of graphene, its potential for chemical applications, especially in organic catalysis and photocatalysis, is a rapidly expanding research area.[7-11] Alongside pristine graphene, graphene-derived materials such as graphene oxide and so-called "multi-layer graphene" have also attracted attention as potential heterogeneous catalysts. For a long time, carbon-based catalysts, or carbocatalysts, have been considered as alternatives to transition metals and have the potential to both reduce the cost of replacing the catalyst (often containing precious metals such as Pt and Ir) and improve the sustainability of industrial reactions.[12] It has also been identified that in a number of catalytic processes, carbon deposited on the solid catalyst surface during reaction can play a key role in providing catalytic active sites or in directing catalytic selectivity. Nanocarbons such as graphene offer the opportunity to create catalytic function using carbon itself as the active element, rather than simply as a supporting medium.[13]

In the last decade, several applications of graphene in heterogeneous catalysis have been reported, for instance the oxygen reduction reaction (ORR),[14-17] the oxidative dehydrogenation of propane[18] and the oxidative coupling of amines to imines[19]. Of particular interest is the dehydrogenation of light alkanes to their corresponding alkenes. Light alkenes such as ethene, propene and butane are vital feedstocks in the chemicals industry, being employed in the manufacture of polymers and plastic, oxygenates and other important compounds. Graphene chemical properties have been investigated by either dissolving graphene fragments in solution, or by using surface science techniques to explore the behaviour of graphene as a two-dimensional crystal.[15, 20] The latter approach is currently a more popular research field, especially in the areas of catalysis and industrial chemistry.[9, 17, 20-21] Despite the increasing popularity of research in this area, there remain a number of uncertainties around the mechanism by which carbon materials catalyse organic transformation. For instance, quinolinic or hydroxyl moieties have been implicated as active sites in the oxidative dehydrogenation of alkanes; however, in the absence of oxygen, and hence these functionalities, carbon catalysts remain capable of promoting dehydrogenation.[14, 17, 22-29] Recently, propane dehydrogenation on defective graphene has been thermodynamically investigated with first-principles methods. The results of this work show that graphene defects do not get poisoned during the dehydrogenation process, although activation energies are not reported.[27] Ethane direct dehydrogenation over carbon nanotubes and reduced graphene oxide has been studied by Bychko and co-authors using scanning electron microscopy, X-ray diffraction and Raman spectroscopy.[26] The authors report that both carbon systems are stable up to 973 K and that ethane and hydrogen are adsorbed on the same active site, therefore adsorbed hydrogen can suppress the rate of dehydrogenation at low temperatures. Understanding the mechanism of reaction allows the design of new catalysts and operating conditions; critical developments given the high energy demands of catalytic dehydrogenation and the typically low selectivities associated with these processes.

The work of the group of McGregor and co-workers[30], in particular, prompts us to explore the observed catalytic activity of nanocarbons with a first-principles theoretical study. While conducting research into the (non-oxidative) dehydrogenation of butane on a metal catalyst, these authors observed the dehydrogenation occurring on a carbon deposit, commonly identified as "coke". The carbonaceous deposit was characterized to be graphitic in nature, but with active site or defects consistent with graphene vacancies.[30]

In this paper, we employ first-principles density functional theory (DFT) methods with van der Waals (vdW) corrections[31] to describe the reaction mechanism of butane dehydrogenation over a graphitic surface with vacancies. The theoretical model of this reaction mechanism not only provides greater insight into catalytic reactions on carbon materials, but also enables us to assess important features of the reaction, for example selectivity. The first-principles model opens the route to tuning the reaction, whether by modifying the catalyst or by changing the reaction conditions. Alongside theoretical studies, complementary adsorption microcalorimetry studies have been conducted to quantify the adsorption energy of butane on the catalytic active coke layer previously described by McGregor *et al*.[22] These measurements provide quantitative values of the heat released upon adsorption against which to benchmark the results of the calculations.

In this study, the substrate has been modelled by a defective graphene layer containing a single atomic vacancy. Previous studies of the reactivity of defects in graphene have suggested that a mono-vacancy is the most reactive defect, and a number of such vacancies are always present on graphene even at room temperature.[32] For this reason, we only considered the mono-vacancy as the reactive site on graphene. The chemistry of graphene is thought to be largely similar to that of graphite.[2] The main advantage of using graphene in this computational study is that it allows us to greatly reduce the number of atoms in the simulation. Additionally, when considering reactions occurring on the surface of coke deposits,

typically only small number of carbon layers are present. Furthermore, the presence of even multiple underlying graphitic layers has little impact on the structure of defects in graphene.[33-35]

2 Experimental and Theoretical Methodology

2.1 Computational Method

Several methods were involved in our exploration of the energy landscape. Both the minima and the transition states connecting these minima have been determined by DFT calculations through the CASTEP[36] code. CASTEP provides both a geometry optimisation method based on the Broyden–Fletcher–Goldfarb–Shanno (BFGS) algorithm and a transition state searching method based on the Linear Synchronous Transit/ Quadratic Synchronous Transit algorithm (LST/QST).[37-38] The OPTIM computer code was also used, coupled with CASTEP, implementing an eigenvector-following (EF) algorithm - a single-ended search method that we employ to find transition states starting from a single geometry (often a local minimum) or for optimising transition states (TS) found with the LST/QST method.[39-41] Convergence testing identified a (4 × 4) cell as sufficiently large to avoid spurious interaction between adjacent vacancies, or indeed between adjacent adsorbed molecules. This coverage corresponds to a vacancy density of 0.012 $Å^{-2}$. The following computational parameters (kinetic energy cutoff and k-point sampling) were firstly converged and then employed for all the calculations reported in this work. The cutoff-energy for the plane wave basis set was 360 eV. The Brillouin zone was sampled with a 2 × 2 × 1 Monkhorst-Pack k-point-grid. The Perdew, Burke, and Ernzerhof (PBE) exchange-correlation functional[42] was utilized with the Tkatchenko-Scheffler (TS) vdW-correction scheme[43] to account for the long-range dispersion force interactions that are dominant in the initial physisorption of butane on graphene. For the electronic convergence, we employ a density-mixing[44-45] approach, with a smearing-

width of 0.1 eV, and set the energy tolerance at 10^{-9} eV/atom. Geometry optimisation calculations were converged to a tolerance of 2×10^{-6} eV/atom and an energy tolerance of 10^{-4} eV for the whole system.

2.2 Adsorption Microcalorimetry

Differential heats of n-butane adsorption were determined at 313 K using a MS70 Calvet Calorimeter (SETRAM). The calorimeter is combined with a custom high vacuum and gas dosing apparatus (volumetric-barometric system), which has been described in detail previously.[46] A custom high-vacuum all-metal sample cell with batch geometry was used in this study.[47] The sample was loaded into the calorimeter cell, and pre-treated at 500 °C for 30 minutes under vacuum, then with 50% H_2 for 30 min prior to degassing 30 minutes under ultra-high vacuum ($p < 3 \quad 10^{-7}$ mbar) achieved using a separate pumping station. Six H_2/de-gas cycles were completed resulting in 180 min exposure to H_2. Subsequently, the cell was cooled to 313 K in vacuum and transferred into the calorimeter. The calorimeter cell was equipped with the volumetric-barometric system. The probe molecule, n-butane, was introduced stepwise into the evacuated cell, with the pressure evolution and the heat signal recorded for each dosing step. The equilibrium pressure increased monotonically with each step from 0.02 mbar after the first step to 86.58 mbar after the final step.

3. Results and Discussion

3.1 Adsorption Microcalorimetry

Figure 1 shows the differential heat of adsorption on coke deposited on VO_x/Al_2O_3 as a function of the quantity of *n*-butane adsorbed. The initial differential heat of adsorption is 0.56 eV. This rapidly decreases with increasing *n*-butane coverage until a coverage of ~0.02 mmol/g, corresponding to a differential heat of adsorption of ~0.4 eV. Above this coverage the rate of decrease slows significantly and ultimately approaches the condensation enthalpy of *n*-butane at 313 K of 0.23 eV. Therefore, this enthalpy

corresponds to that of a "liquid" monolayer on the surface, and the experimentally measured heats of adsorption tend to this value. After the surface becomes saturated, multilayer adsorption will commence at which point we would no longer be investigating the interaction of the adsorbate with the surface. The relatively higher enthalpies observed at low coverage likely correspond to adsorption of *n*-butane at defect sites on the coke surface. The monotonic nature of the decrease in enthalpy with increasing coverage indicates that no reactive event, such as isomerisation of the hydrocarbon, occur following adsorption.[47]

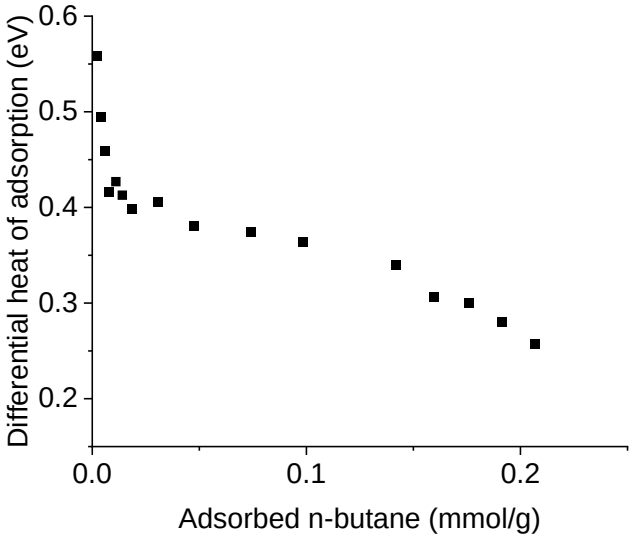

Figure 1 Differential heat of adsorption of n-butane at 313 K on a carbonaceous overlayer deposited on VO_x/Al_2O_3.

3.1 Physisorption

The first step of the reaction - the physisorption of butane on graphene - requires the molecule and surface to be in close proximity, and the orientation of the impinging molecule is likely to be of some importance.[48-52] In order to determine the structure of the physisorbed state and the depth of the physisorption well, a series of geometry optimisations were performed with butane initially positioned at 3 Å from the vacancy. Butane was found to physisorb, and Figure 2 shows two possible orientations for

the optimised geometry. The vertical orientation has an adsorption energy of 0.23 eV with a calculated minimum height of 3.2 Å (the minimum distance between any carbon atom in the molecule and the plane of the graphene sheet). The horizontal orientation adsorbs with a higher adsorption energy of 0.40 eV and a minimum height of 3.3 Å. Rotating the physisorbed butane about its longest molecular axis does not significantly affect the adsorption energy for the horizontally physisorbed state. The higher adsorption energy for the horizontal state (compared with the vertical state) can be understood from the nature of the vdW correction added to the DFT calculation - in the horizontal geometry the atoms in the molecule are generally closer to the sheet and therefore the vdW interactions (included in a pairwise manner) are correspondingly stronger.[53-55] For intermediate orientations, where the butane molecule lies at an angle between vertical and horizontal, the adsorption energy varies smoothly between 0.23 eV and 0.40 eV, in excellent agreement with the microcalorimetry results (Figure 1).

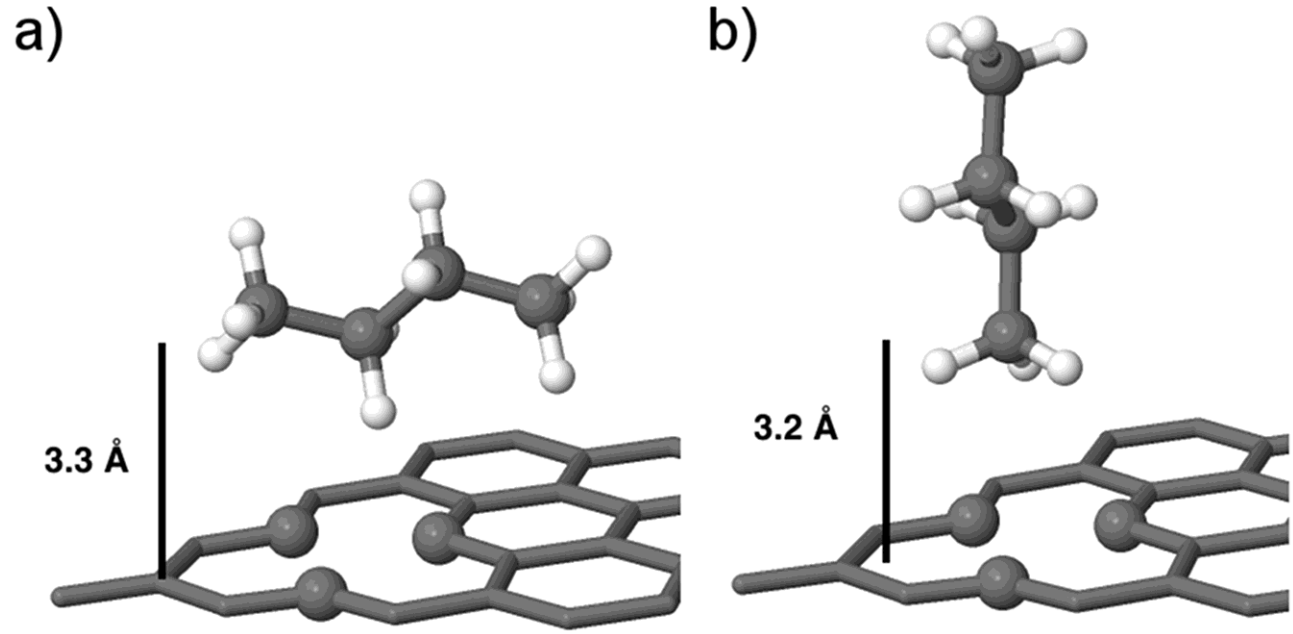

Figure 2 Physisorbed butane above the graphene mono-vacancy in (a) horizontal, and (b) vertical orientations. Adsorption energies are 0.40 eV in the horizontal orientation, and 0.23 eV in the vertical.

3.2 First Deprotonation

In order to calculate the reaction barrier for the first deprotonation reaction, which ends with a hydrogen atom adsorbed on the vacancy and a 1-butyl radical physisorbed on graphene, we employ the eigenvector following (EF) algorithm,[39-41] an efficient single-ended TS search method that determines the transition state for a reaction by starting from a single geometry. The single-ended search is achieved by following the least-steep path uphill (corresponding to the lowest energy eigenvector of the Hessian,[40, 56] the matrix of second derivatives of the energy with respect to geometry) on the energy landscape from the local minimum to a transition state. There are two environments for hydrogen atoms on a butane molecule - the

first is attached to one of the primary carbon atoms of butane (the termini of the alkane) whereas the other is attached to one of the secondary carbon atoms (in the middle of the alkane).

Figure 3 Transition state showing the removal of a hydrogen atom from a primary carbon atom of butane by the graphene mono-vacancy, red arrows showing the reaction vector. The transition state has an energy 0.56 eV higher than the vertically physisorbed state (Figure 2(b)), and 0.73 eV higher than the horizontally physisorbed state (Figure 2(a)). Figure 3 also shows the resulting geometry from a successful transition state search for removing a hydrogen atom from a primary carbon atom, starting from a vertically physisorbed state similar to that depicted in Figure 2(b). The transition state has an energy of 0.33 eV relative to gas-phase butane and a pristine vacancy site, which is 0.56 eV above that of the initial vertically physisorbed state, or 0.73 eV above that of the (lowest energy) horizontally physisorbed state. The resulting transition state structure shows that butane moves slightly closer to the surface and the leaving hydrogen lies at an intermediate distance from the primary carbon atom of the molecule and one of the carbon atoms in the vacancy. The distance from this proton to the nearest graphene carbon atom is 1.3 Å, while the breaking C-H bond is 1.4 Å in length. The Hessian eigenvector with lowest eigenvalue,[40] corresponding to the direction of the reaction co-ordinate at the transition state, is marked with red arrows in 3, revealing the movement of the hydrogen between the adsorbate and vacancy.

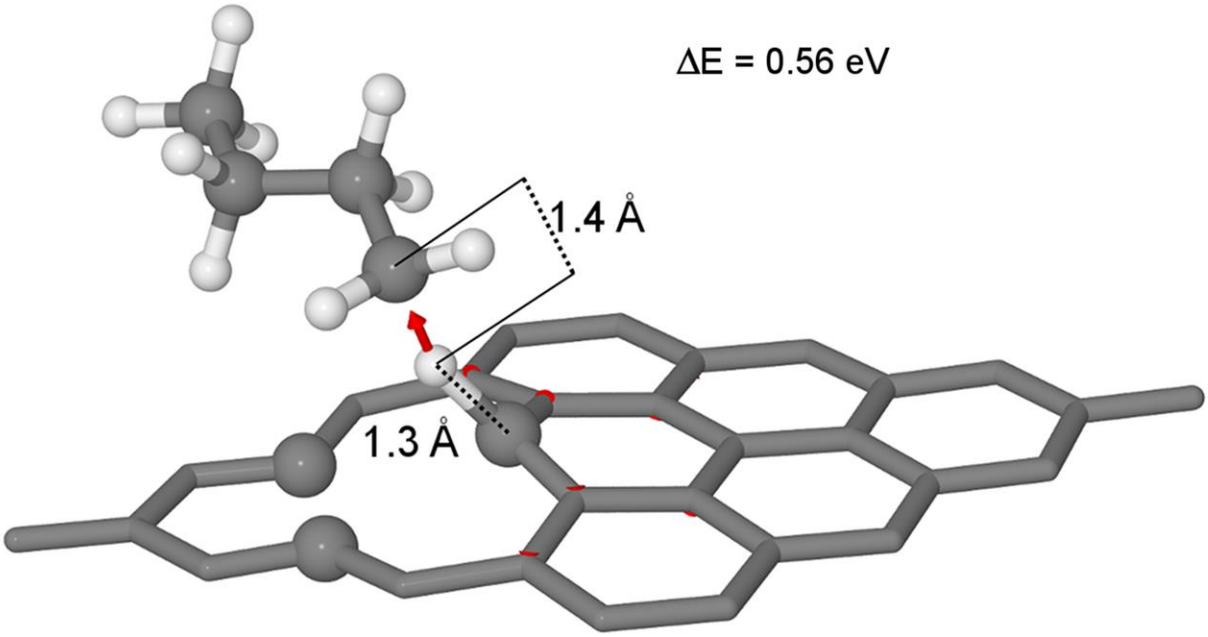

Figure 3 Transition state showing the removal of a hydrogen atom from a primary carbon atom of butane by the graphene mono-vacancy, red arrows showing the reaction vector. The transition state has an energy 0.56 eV higher than the vertically physisorbed state (Figure 2(b)), and 0.73 eV higher than the horizontally physisorbed state (Figure 2(a)).

Figure 4 shows the geometry for a transition state search in which a hydrogen atom is removed from one of the secondary carbon atoms of butane. The transition state has an energy of 0.20 eV, relative to gas-phase butane and a pristine vacancy site, which is 0.59 eV above that of the horizontal physisorbed geometry (from which the search was started). The calculated TS shows a similar structure to the TS for the deprotonation of a primary carbon (Figure 3), with a C-H distance of 1.4 Å for the breaking bond, and of 1.3 Å between the leaving hydrogen atom and the nearest carbon atom in the graphene sheet.

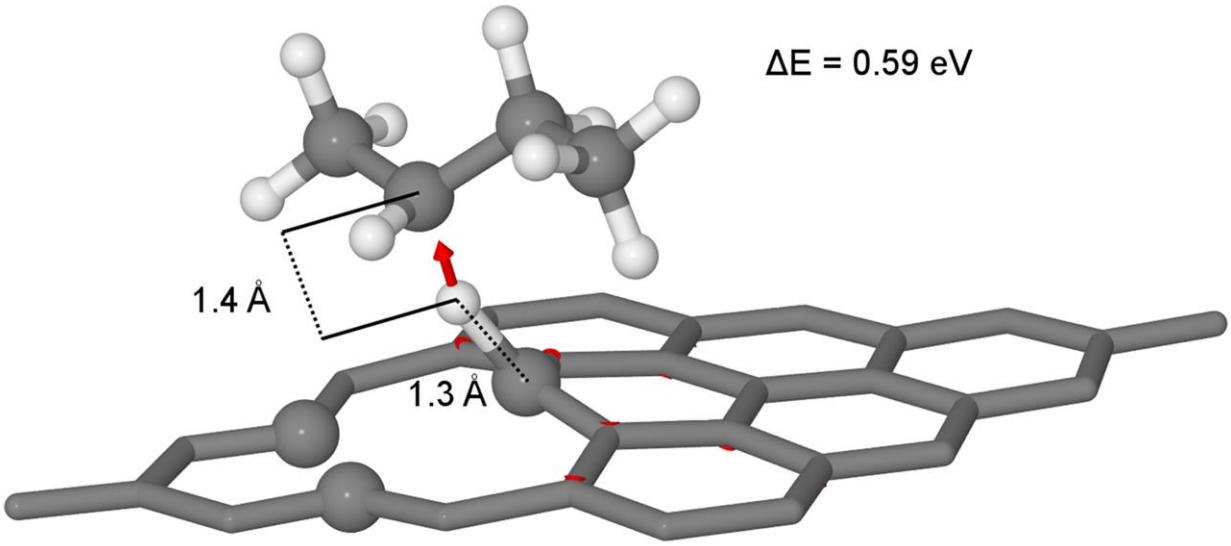

Figure 4 Transition state (TS) showing the removal of a hydrogen atom from one of the secondary carbons of butane by the graphene mono-vacancy, red arrows showing the reaction vector. The transition state has an energy 0.43 eV higher than the vertically physisorbed state (Figure 2(b)), and 0.59 eV higher than the horizontally physisorbed state (Figure 2(a)).

3.3 Chemisorption

The transition states shown in Figure 3 and Figure 4 connect physisorbed butane with a physisorbed butyl radical (and a chemisorbed hydrogen atom located on the vacancy). There are then two possible binding sites where the butyl radical could react with the vacancy, following removal of the first hydrogen atom. Since a single bond can form between a carbon atom in the vacancy and the molecule, the butyl radical can either react with the carbon atom on which the hydrogen atom has adsorbed or with one of the two unoccupied carbon atoms belonging to the vacancy (Figure 3 and 4).[57] We calculated the energy for

both adsorption geometries and found that butyl bonded to the same carbon atom as the hydrogen atom is higher in energy by 0.29 eV than butyl bonded to a different carbon atom of the vacancy. Choosing to focus only on the latter possibility, therefore, Figure 5 shows the optimised geometries of 1-butyl and 2-butyl chemisorbed to the vacancy. The energy difference between these two structures is 0.15 eV, the 1-butyl configuration being the more stable, and in both cases there is substantial modification of the local structure at the vacancy site. Transition state searches aiming to link these chemisorbed states to physisorbed butyl radical geometries obtained as endpoints of the first deprotonation step proved fruitless, demonstrating that chemisorption of the butyl radical is essentially barrierless.

Several further adsorption geometries for the chemisorbed butyl moieties were then explored by rotating each around its chemisorption bond, so that it extended variously over either the vacancy or the graphene sheet. The maximum change in adsorption energy was found to be less than 1 meV, indicating that rotational motion of either chemisorbed butyl moiety would be facile.

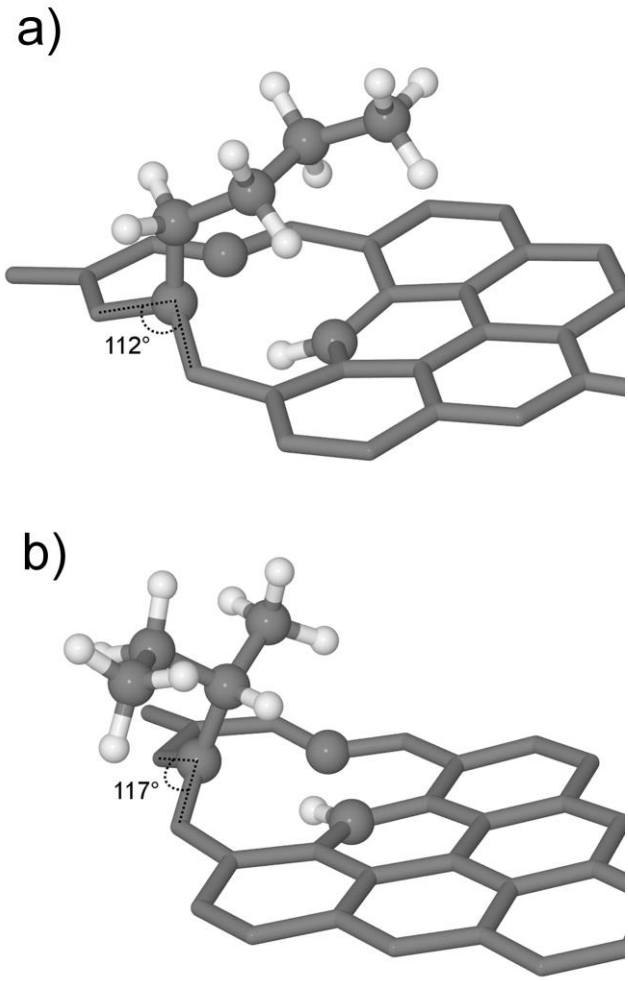

Figure 5 Optimized structure of chemisorbed butyl, with a single hydrogen atom removed from (a) a primary carbon atom, forming a 1-butyl moiety, or (b) a secondary carbon atom, forming a 2-butyl moiety. The energy difference between these structures is 0.15 eV, with the 1-butyl moiety the more stable structure.

3.4. Second Deprotonation

Figure 5 shows butyl moieties bonded to the vacancy, with a single hydrogen atom removed from the molecule in each case and bonded nearby. To proceed forward in the reaction, another hydrogen atom must be removed to create an adsorbate with the stoichiometry of butene. Since there are two possible geometries resulting from the removal of the first hydrogen atom, corresponding to whether it has been removed from either a primary or a secondary carbon, there are necessarily three distinct configurations (see Figure 7) resulting from the removal of a second hydrogen atom, depending on which order the hydrogen atoms are removed from the original butane. Figure 6 (c) shows the geometry of a TS that leads to the removal of a second hydrogen atom from a 1-butyl moiety. In this case, the second hydrogen atom is removed from a secondary carbon of the original butane molecule, while the first hydrogen atom was removed from a primary carbon atom. The calculated activation barrier corresponding to the transition state for this reaction is 0.67 eV. Beyond the transition state, the hydrogen atom will continue to displace in the direction of the reaction vector, eventually bonding to one of the carbon atoms at the vacancy. The highly reactive butyl radical immediately forms a second bond to that same carbon atom, forming a chemisorbed cyclic intermediate (shown in Figure 6(c)).

If, instead, the first hydrogen atom removed from butane left from a secondary carbon atom, there will be two possible locations from which to remove the second hydrogen atom - either from a primary carbon atom (Figure 6(a)) or from another secondary carbon atom (Figure 6(b)). The TS in the first case involves an activation barrier of 0.81 eV, whereas the activation barrier in the second case is 0.54 eV. In both cases, the hydrogen atom follows the reaction vector at the transition state to bond with a carbon atom at the vacancy, while the chemisorbed butyl moiety forms a second bond with that same carbon atom to produce, once again, a chemisorbed cyclic intermediate.

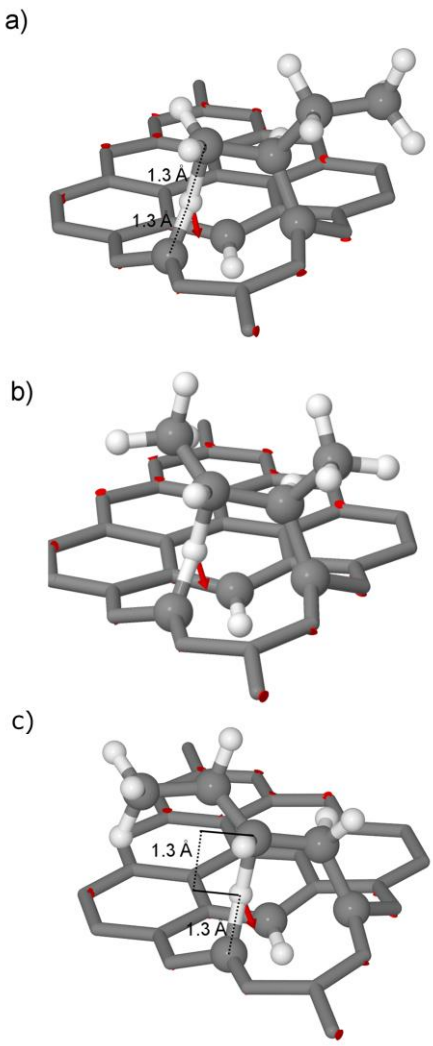

Figure 6 Transition states (TS) for the removal of a second hydrogen atom (a) from a primary carbon atom of vacancy-adsorbed 2-butyl; (b) TS for the removal of a hydrogen atom from a secondary carbon atom of vacancy-adsorbed 2-butyl. The activation barrier for the former reaction is 0.81 eV, while for the latter it is 0.54 eV (TS energies of -2.83 eV and -2.93 eV, relative to respective products, but-1-ene and but-2-ene). (c) TS for removal of a hydrogen atom from a secondary carbon atom of 1-butyl. This TS has an energy of -3.12 eV relative to gas-phase butane and a pristine vacancy site, which corresponds to an activation barrier of 0.67 eV from a starting point of vacancy-chemisorbed 1-butyl and a single adjacent hydrogen atom.

Following the removal of two hydrogen atoms from butane, both they and the remnant moiety are bonded to the vacancy site. Each departed hydrogen atom is bonded to a different carbon atom, while the molecule has replaced each with a bond to a vacancy carbon atom and forms a cyclic intermediate with either an ethyl group (Figure 7(a) and (c)) or two methyl groups (Figure 7(b)). Figure 7(c) shows the product of the deprotonation depicted in Figure 6(c), originating from a 1-butyl intermediate. Figures 7(a) and 7(b) show, respectively, the products of the deprotonations depicted in Figures 6(a) and 6(b), originating from a 2-butyl intermediate. These three structures differ in energy by less than 0.05 eV, and indeed the only difference between the geometries presented in Figure 7(a) and 7(c) is the position of the hydrogen atoms bonded to the vacancy. We therefore explored that how hydrogen atoms can diffuse across the vacancy via a reaction path connecting these two states, obtaining the transition state presented in Figure 8. If the diffusing hydrogen atom is initially in the state represented in Figure 7(a), the activation barrier presented by the transition state is 0.40 eV, whereas if the initial configuration is that represented in Figure 7(b) the activation barrier is 0.44 eV. An activation barrier smaller than around 0.5 eV indicates that the hydrogen atoms adsorbed on the vacancy are highly mobile, even at room temperature.

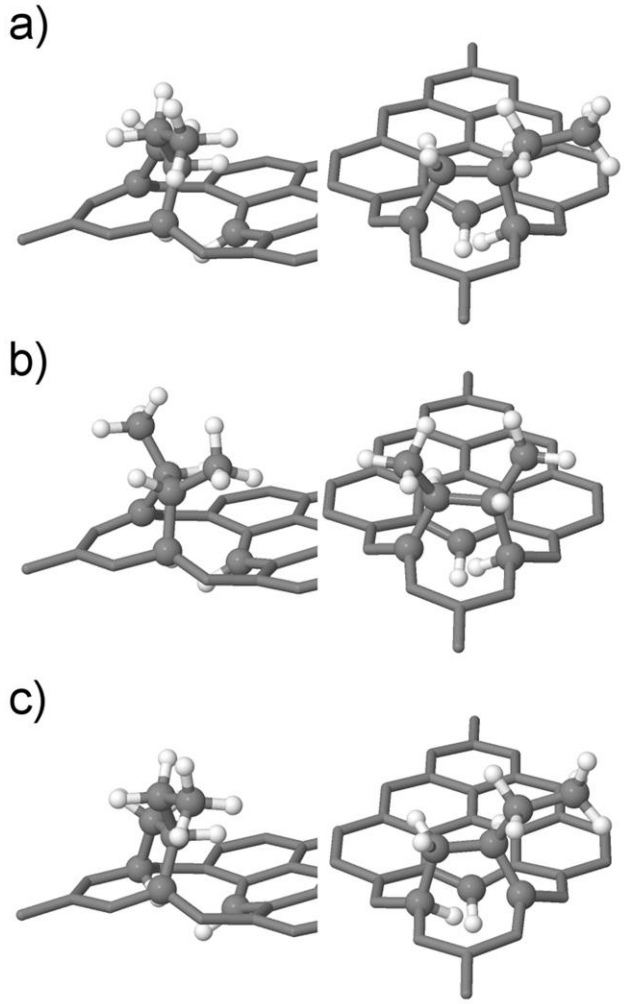

Figure 7 Products of double deprotonation, showing cyclic intermediates bonded twice over the graphene mono-vacancy. In (a) we show the product from deprotonation of chemisorbed 1-butyl (-5.43 eV relative to but-1ene), in (b) the product from deprotonation of 2-butyl at a secondary carbon atom (-5.32 eV), and in (c) the product from deprotonation of 2-butyl at a primary carbon atom (-5.47 eV relative to but-1ene).

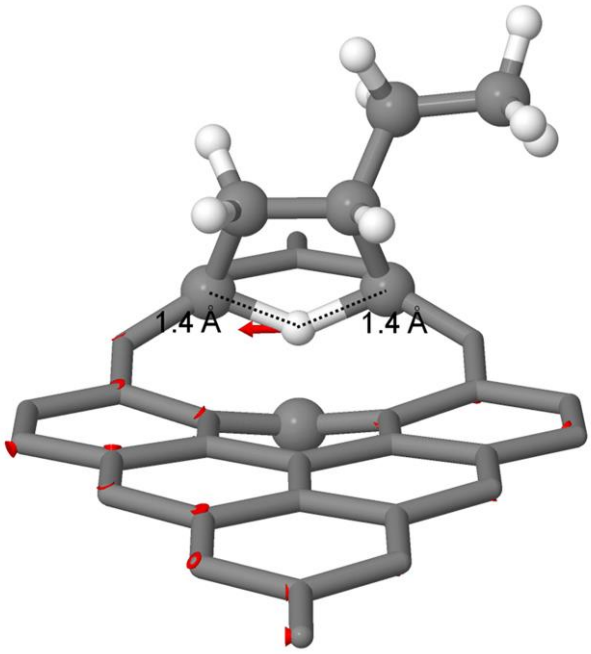

Figure 8 Transition state for hydrogen atom diffusion across the vacancy. The transition state connects the ground-state geometries shown in Figure 7 (a) and (c). The activation barriers from these minima are 0.40 eV and 0.44 eV, respectively.

3.5. Butene Desorption

Ignoring, for a moment, the two hydrogen atoms bound directly to the vacancy site, the cyclic intermediates shown in Figure 7 can be thought of as chemisorbed but-1-ene (Figs. 7(a) and 7(c)) and but-2-ene (Figure 7(b)), albeit we must take care to stress that the double bonds implied by such nomenclature are actually just single bonds in these adsorbed configurations. Nevertheless, we shall risk describing them as alkenes, noting that scission of two C-C adsorption bonds in each case would result in desorption of genuine but-1-ene or but-2-ene respectively. In order that vacancy sites are not swiftly poisoned, however, it will also be necessary for the deposited hydrogen atoms to have a route via which to depart, but we defer consideration of this to the following section.

For the moment, we note that the pathway for cleavage of two C-C bonds and desorption of butene can be either symmetric (both bonds break simultaneously) or asymmetric (the bonds break sequentially). Perhaps unsurprisingly, only asymmetrical transition states were found by the single-ended TS searches. Figure 9 shows the resulting geometries and reaction vectors of these transition states. Starting from the configuration shown in Figure 7(a), we located the TS depicted in Figure 9(a), with an activation barrier for the desorption amounting to but-1-ene of 2.39 eV (-1.24 eV relative to gas-phase butane and a pristine vacancy site), while starting from a configuration equivalent to that shown in Figure 7(c) we located the TS depicted in Figure 9(c), with an activation barrier for the desorption of but-1-ene amounting to 2.57 eV (-1.28 eV relative to gas-phase butane and a pristine vacancy site). Desorption of but-2-ene, on the other hand, involves the TS depicted in Figure 9(b), obtained from the starting geometry shown in Figure 7(b), with an activation barrier amounting to 2.47 eV (-1.39 eV relative to gas-phase butane and a pristine vacancy site).

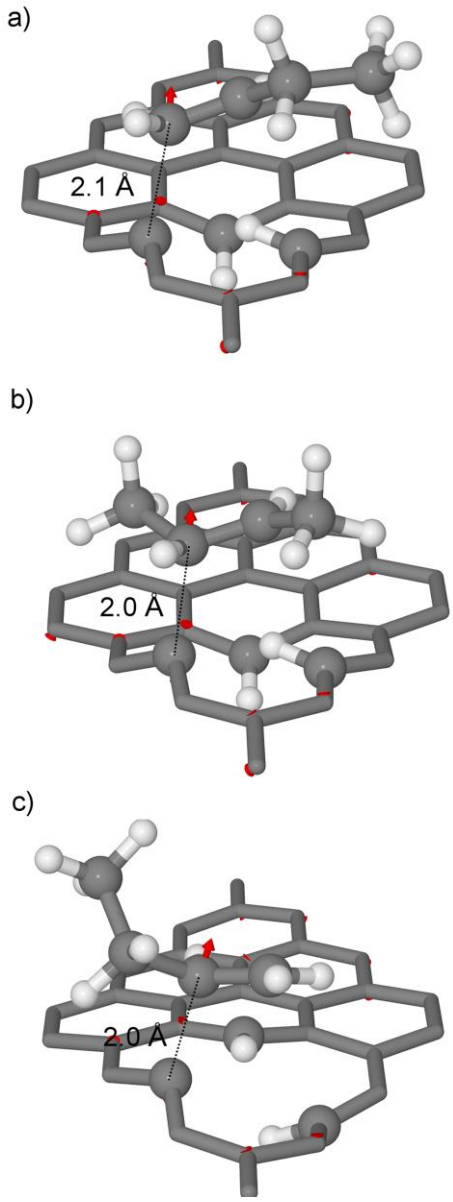

Figure 9 Transition states for the desorption of butene from a vacancy with two hydrogen atoms bonded to the vacancy. In (a) we show the desorption of but-1-ene via an activation barrier of 2.39 eV, in (c) the desorption of but-1-ene via an activation barrier of 2.57 eV, and in (b) the desorption of but-2-ene via an activation barrier of 2.47 eV (i.e. TS energies of -3.04 eV, -2.85 eV and -2.91 eV, respectively, relative to gas-phase butane and a pristine vacancy site).

3.6. Hydrogen Desorption

As mentioned in passing above, for the butane dehydrogenation mechanism describe here to be catalytic, the pristine mono-vacancy must be recovered at the end of the reaction, either through desorption of H_2 or via diffusion of H across the graphene sheet. The latter process is highly unlikely, however, since we calculate H atoms to be more stable by ~2 eV at the vacancy than on non-defective graphene. We assume here, for simplicity, that hydrogen desorbs, and that it does so after the newly formed butene molecule has already departed.

Figure 10 shows the four possible configurations in which hydrogen can be adsorbed on a vacancy. The monohydride-cis configuration is the lowest in energy, by a small margin, relative to the monohydride-trans configuration, and by a large margin from the two dihydride geometries. The monohydride-cis configuration can easily convert into monohydride-trans, with a calculated activation barrier of less than 0.01 eV. A much higher activation barrier of 0.40 eV was found for conversion of the dihydride-trans configuration to the dihydride-cis geometry.

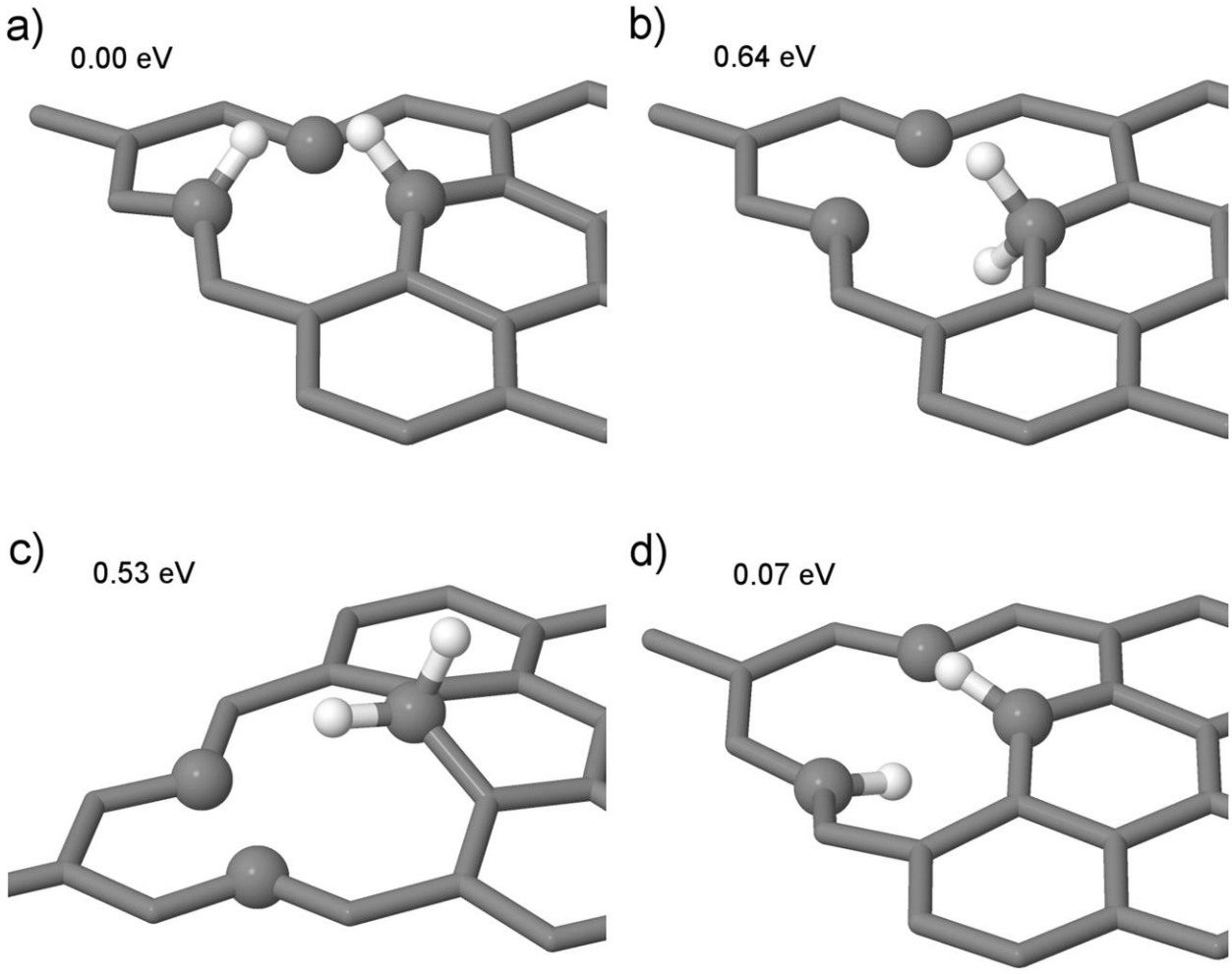

Figure 10 Four different configurations of two hydrogen atoms bonded to the graphene vacancy, with relative energies reported relative to the most stable configuration. We label these as (a) monohydride-cis, (b) dihydride-trans, (c) dihydride-cis, and (d) monohydride-trans, according to the number of hydrogen atoms attaching to the involved carbon atom(s) and the disposition of these atoms relative to the two side of the graphene sheet.

From the minimum energy configuration (monohydride-cis), the recombinative desorption of H_2 from the graphene vacancy proceeds via a TS with an activation barrier of 3.11 eV (Figure 1). This is broadly comparable with the value calculated by Jiang et al [58] (3.63 eV), with the difference probably due to the choice of dispersion correction employed. Although this activation barrier is rather high, and indeed quite a bit higher than that involved in liberating butene from the vacancy, it is perfectly reasonable to expect desorption to occur at the elevated temperatures (c.900 K and above) employed in the work of McGregor et al [22] on coke. Notably, those authors note that their catalyst gradually deactivates over time when operated at 873 K, but that the opposite is true at higher temperatures, and this is likely quite consistent with activated desorption of H_2 from low-coordination sites (such as the graphene mono-vacancy or analogous sites in carbonaceous coke).

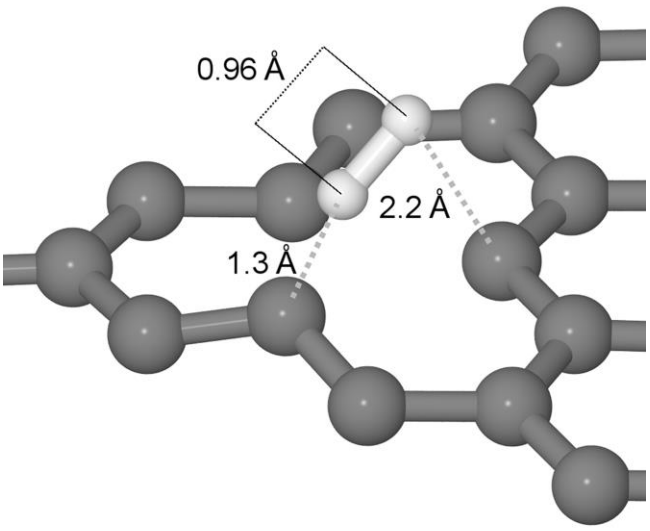

Figure 11 Transition state structure for the associative desorption of hydrogen (H_2) from the graphene mono-vacancy. The desorption reaction has an activation barrier of 3.11 eV above the initial state in which two protons are chemisorbed on the two adjacent carbons of the vacancy.

3.7 Reaction Pathway

Figure 12 shows the energies and geometries for the two possible energy pathways. Each path leads to one of the two possible products, but-1-ene or but-2-ene. The states in each path are unique, including different initial orientations for butane physisorbed above the vacancy. If the butane molecule approaches the vacancy end-on, but-1-ene is formed, but if the butane is initially parallel to the vacancy it is possible to form but-2-ene. Indeed, all the intermediate activation energies are rather comparable from one pathway to the other and are rather unlikely to generate any substantial selectivity between the two possible products at the high temperatures employed in the experiments of McGregor and co-workers[22]. Nevertheless, these authors reported almost complete conversion to but-1-ene or 1,3-butadiene (the latter presumably created by dehydrogenation of the former in a second catalytic encounter) and practically no formation of but-2-ene. Our calculations suggest that this high selectivity cannot be explained by substantial differences in the catalytic pathway followed after initial adsorption, but must instead arise as a result of steric considerations in the initial approach of butane to the active vacancy site. The molecule possesses six hydrogen atoms (attached to primary carbon atoms) that could react with the vacancy and lead into the but-1-ene pathway, but only four (attached to secondary carbon atoms) that could react and lead into the but-2-ene pathway. Furthermore, the spatial distribution of these hydrogen atoms may well make the former set more tolerant of molecular misalignment in the approach to the vacancy. That is, the range of orientations that yield an initial reaction involving one of the hydrogen atoms from the mid-section of the molecule may well be considerably more limited that the range consistent with initial reaction involving a hydrogen atom attached to one of the termini of the molecule. Note that at elevated temperature, physisorption of the molecule will be negligible, so the opportunity for reorientation above the vacancy may similarly be neglected.

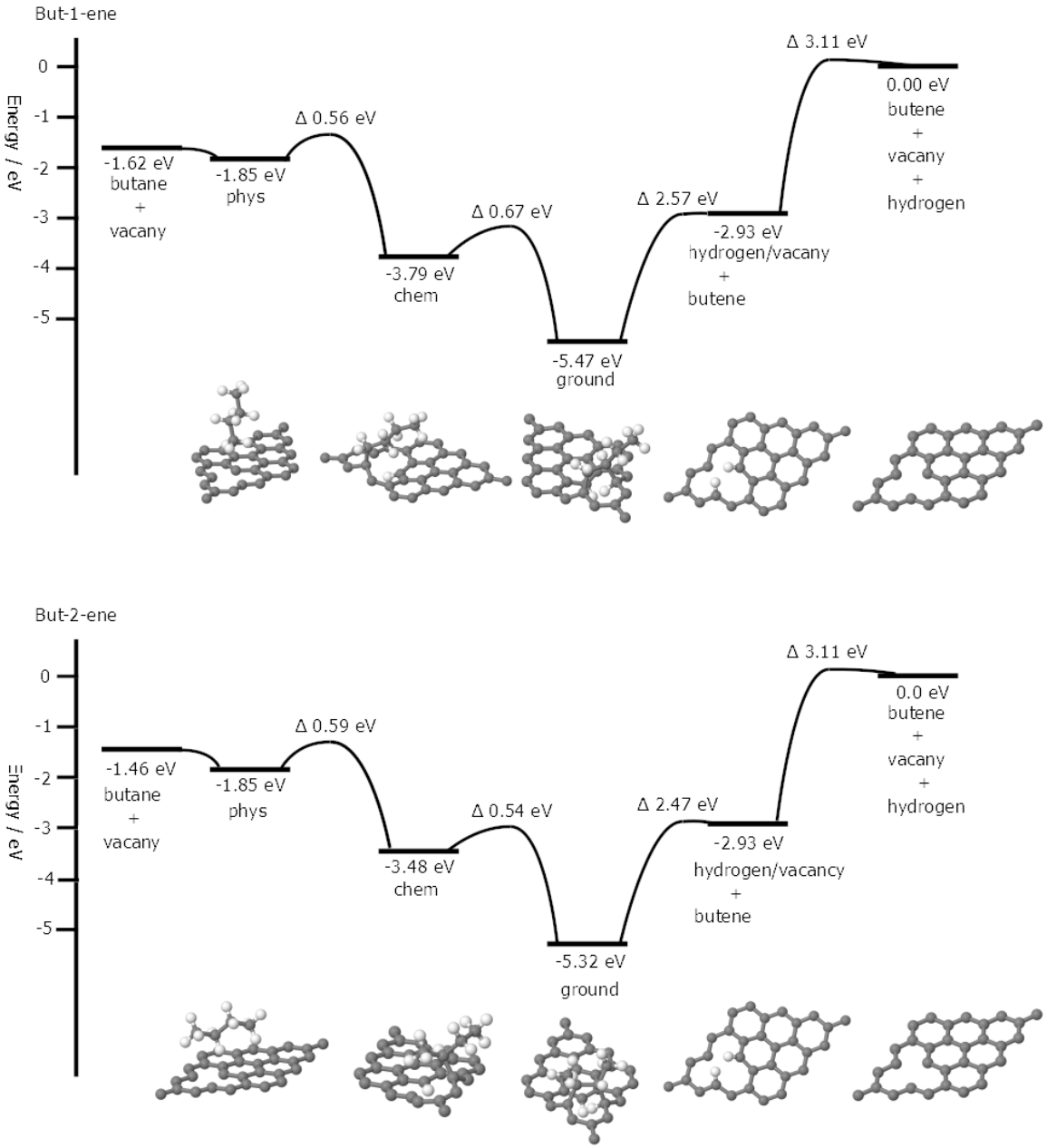

Figure 12 Mechanism for the dehydrogenation of butane to but-1-ene (top panel) and but-2-ene (lower panel). The barrier height (eV) separating the minimum energy configurations is indicated with Δ.

4. Conclusions

The complete reaction pathway for the catalytic conversion of butane to butene has been calculated. The reaction can be broken down into several steps, leading to the creation of butene and the recovery of the catalytic active site, namely the pristine vacancy. The first step is the physisorption of butane above the vacancy. For this step, the results of the dispersion-corrected DFT calculations closely match our microcalorimetry measurements. The butane physisorption is followed by deprotonation and chemisorption in which the resulting butyl moiety forms a bond with one of the dangling bonds of the vacancy. Further deprotonation and chemisorption lead to a cyclic intermediate that can be (loosely) viewed as adsorbed butene, with the precise isomer dictated by the order of deprotonation. The lowest energy of the overall reaction mechanism is reached when both liberated hydrogen atoms and the cyclic intermediate are bound to the vacancy. Finally, butene desorbs from the vacancy into the gaseous state by sequentially breaking two C-C bonds. To recover the pristine vacancy, renewing the catalytic active site, both hydrogen atoms must leave the vacancy and this appears to be the most energetically onerous step of the entire mechanism. Pathways to the formation of both but-1-ene and but-2-ene have been described, and shown to be energetically rather similar. The experimentally observed selectivity towards but-1-ene and 1,3-butadiene, rather than but-2-ene, can therefore only be explained by preferential entry into the pathway that begins with deprotonation at a primary carbon atom rather than a secondary one. This, in turn, strongly suggests that the observed selectivity stems from the steric advantage enjoyed by an end-on approach of butane impinging upon the active vacancy site, compared with a sideways-on approach.

Acknowledgements

MS would like to thank the Royal Society for his University Research Fellowship. We are grateful to Prof. David Wales for many insightful discussions.

References

1. Novoselov, K. S.; Geim, A. K.; Morozov, S. V.; Jiang, D.; Zhang, Y.; Dubonos, S. V.; Grigorieva, I. V.; Firsov, A. A., Electric Field Effect in Atomically Thin Carbon Films. *Science* **2004,** *306* (5696), 666--669.
2. Geim, A. K., Graphene: Status and Prospects. *Science* **2009,** *324* (5934), 1530-1534.
3. Young, A. F.; Kim, P., Quantum interference and Klein tunnelling in graphene heterojunctions. *Nature Physics* **2009,** *5* (3), 222--226.
4. Stander, N.; Huard, B.; Goldhaber-Gordon, D., Evidence for Klein Tunneling in Graphene \$p\backslashmathrm\\backslashtext\-\\n\$ Junctions. *Phys. Rev. Lett.* **2009,** *102* (2), 26807.
5. Castro Neto, A. H.; Guinea, F.; Peres, N. M. R.; Novoselov, K. S.; Geim, A. K., The electronic properties of graphene. *Reviews of Modern Physics* **2009,** *81* (1), 109.
6. Geim, A. K.; Novoselov, K. S., The rise of graphene. *Nat Mater* **2007,** *6* (3), 183-191.
7. Li, H. B.; Xiao, J. P.; Fu, Q.; Bao, X. H., Confined catalysis under two-dimensional materials. *Proceedings of the National Academy of Sciences of the United States of America* **2017,** *114* (23), 5930-5934.
8. Hu, M. C.; Yao, Z. H.; Wang, X. Q., Graphene-Based Nanomaterials for Catalysis. *Industrial & Engineering Chemistry Research* **2017,** *56* (13), 3477-3502.
9. Deng, D. H.; Novoselov, K. S.; Fu, Q.; Zheng, N. F.; Tian, Z. Q.; Bao, X. H., Catalysis with two-dimensional materials and their heterostructures. *Nature Nanotechnology* **2016,** *11* (3), 218-230.
10. Machado, B. F.; Serp, P., Graphene-based materials for catalysis. *Catalysis Science & Technology* **2012,** *2* (1), 54-75.
11. Huang, C. C.; Li, C.; Shi, G. Q., Graphene based catalysts. *Energy & Environmental Science* **2012,** *5* (10), 8848-8868.
12. Navalon, S.; Dhakshinamoorthy, A.; Alvaro, M.; Garcia, H., Carbocatalysis by graphene-based materials. *Chem. Rev.* **2014,** *114* (12), 6179--212.
13. Su, D. S.; Perathoner, S.; Centi, G., Nanocarbons for the Development of Advanced Catalysts. *Chem. Rev.* **2013,** *113* (8), 5782-5816.
14. Hu, C. G.; Dai, L. M., Carbon-Based Metal-Free Catalysts for Electrocatalysis beyond the ORR. *Angew. Chem.-Int. Edit.* **2016,** *55* (39), 11736-11758.
15. Ambrosi, A.; Chua, C. K.; Latiff, N. M.; Loo, A. H.; Wong, C. H. A.; Eng, A. Y. S.; Bonanni, A.; Pumera, M., Graphene and its electrochemistry - an update. *Chem. Soc. Rev.* **2016,** *45* (9), 2458-2493.
16. Dai, L. M.; Xue, Y. H.; Qu, L. T.; Choi, H. J.; Baek, J. B., Metal-Free Catalysts for Oxygen Reduction Reaction. *Chem. Rev.* **2015,** *115* (11), 4823-4892.

17. Wang, D. W.; Su, D. S., Heterogeneous nanocarbon materials for oxygen reduction reaction. *Energy & Environmental Science* **2014,** *7* (2), 576-591.
18. Tang, S.; Cao, Z., Site-dependent catalytic activity of graphene oxides towards oxidative dehydrogenation of propane. *Physical Chemistry Chemical Physics* **2012,** *14* (48), 16558-16565.
19. Su, C.; Acik, M.; Takai, K.; Lu, J.; Hao, S.-j.; Zheng, Y.; Wu, P.; Bao, Q.; Enoki, T.; Chabal, Y. J.; Ping Loh, K., Probing the catalytic activity of porous graphene oxide and the origin of this behaviour. *Nature Communications* **2012,** *3*, 1298.
20. Kong, X. K.; Chen, C. L.; Chen, Q. W., Doped graphene for metal-free catalysis. *Chem. Soc. Rev.* **2014,** *43* (8), 2841-2857.
21. Zheng, Y.; Jiao, Y.; Zhu, Y. H.; Li, L. H.; Han, Y.; Chen, Y.; Du, A. J.; Jaroniec, M.; Qiao, S. Z., Hydrogen evolution by a metal-free electrocatalyst. *Nature Communications* **2014,** *5*.
22. Lawrence, R. A.; Gante, N.; Sacchi, M., Reduction of NO on chemically doped, metal-free graphene. *Carbon Trends* **2021,** *5*, 100111.
23. Chen, H.; Zhu, X.; Huang, H.; Wang, H.; Wang, T.; Zhao, R.; Zheng, H.; Asiri, A. M.; Luo, Y.; Sun, X., Sulfur dots-graphene nanohybrid: a metal-free electrocatalyst for efficient N2-to-NH3 fixation under ambient conditions. *Chem. Commun. (Cambridge, U. K.)* **2019,** *55* (21), 3152-3155.
24. Primo, A.; Parvulescu, V.; Garcia, H., Graphenes as Metal-Free Catalysts with Engineered Active Sites. *The Journal of Physical Chemistry Letters* **2017,** *8* (1), 264-278.
25. Nabid, M. R.; Bide, Y.; Fereidouni, N., Boron and nitrogen co-doped carbon dots as a metal-free catalyst for hydrogen generation from sodium borohydride. *New J. Chem.* **2016,** *40* (10), 8823-8828.
26. Bychko, I.; Abakumov, A.; Nikolenko, A.; Selyshchev, O. V.; Zahn, D. R. T.; Khavrus, V. O.; Tang, J. G.; Strizhak, P., Ethane Direct Dehydrogenation over Carbon Nanotubes and Reduced Graphene Oxide. *Chemistryselect* **2021,** *6* (34), 8981-8984.
27. Ukpong, A. M., Ab initiostudies of propane dehydrogenation to propene with graphene. *Mol. Phys.* **2020,** *118* (24), 22.
28. Li, S. M.; Wang, W. P.; Liu, X.; Zeng, X. L.; Li, W. X.; Tsubaki, N.; Yu, S., Nitrogen-doped graphene nanosheets as metal-free catalysts for dehydrogenation reaction of ethanol. *Rsc Advances* **2016,** *6* (16), 13450-13455.
29. Collett, C. H.; McGregor, J., Things go better with coke: the beneficial role of carbonaceous deposits in heterogeneous catalysis. *Catalysis Science & Technology* **2016,** *6* (2), 363-378.
30. McGregor, J.; Huang, Z.; Parrott, E. P. J.; Zeitler, J. A.; Nguyen, K. L.; Rawson, J. M.; Carley, A.; Hansen, T. W.; Tessonnier, J.-P.; Su, D. S.; Teschner, D.; Vass, E. M.; Knop-Gericke, A.; SchlÃ¶gl, R.; Gladden, L. F., Active coke: Carbonaceous materials as catalysts for alkane dehydrogenation. *J. Catal.* **2010,** *269* (2), 329-339.
31. Sacchi, M.; Singh, P.; Chisnall, D. M.; Ward, D. J.; Jardine, A. P.; Allison, B.; Ellis, J.; Hedgeland, H., The Dynamics of Benzene on Cu(111): a Combined Helium Spin Echo and Dispersion-Corrected DFT Study into the Diffusion of Physisorbed Aromatics on Metal Surfaces. *Faraday Discuss.* **2017,** *204*, 471-485
32. Denis, P. A.; Iribarne, F., Comparative Study of Defect Reactivity in Graphene. *J. Phys. Chem. C* **2013,** *117* (Copyright (C) 2013 American Chemical Society (ACS). All Rights Reserved.), 19048-19055.
33. Palacios, J. J.; Yndurain, F., Critical analysis of vacancy-induced magnetism in monolayer and bilayer graphene. *Physical Review B Condensed Matter and Materials Physics* **2012,** *85* (Copyright (C) 2013 American Chemical Society (ACS). All Rights Reserved.), 245443/1-245443/8.

34. Ugeda, M. M.; Brihuega, I.; Hiebel, F.; Mallet, P.; Veuillen, J.-Y.; Gómez-Rodríguez, J. M.; Ynduráin, F., Electronic and structural characterization of divacancies in irradiated graphene. *Physical Review B* **2012,** *85* (12), 121402.
35. Ugeda, M. M.; Brihuega, I.; Guinea, F.; Gómez-Rodríguez, J. M., Missing Atom as a Source of Carbon Magnetism. *Phys. Rev. Lett.* **2010,** *104* (9), 96804.
36. Clark, S. J.; Segall, M. D.; Pickard, C. J.; Hasnip, P. J.; Probert, M. J.; Refson, K.; Payne, M. C., First principles methods using CASTEP. *Zeitschrift Fur Kristallographie* **2005,** *220* (5-6), 567-570.
37. Pfrommer, B. G.; Côté, M.; Louie, S. G.; Cohen, M. L., Relaxation of Crystals with the Quasi-Newton Method. *Journal of Computational Physics* **1997,** *131* (1), 233-240.
38. Govind, N.; Petersen, M.; Fitzgerald, G.; King-Smith, D.; Andzelm, J., A generalized synchronous transit method for transition state location. *Computational Materials Science* **2003,** *28* (2), 250-258.
39. Kumeda, Y.; Wales, D. J.; Munro, L. J., Transition states and rearrangement mechanisms from hybrid eigenvector-following and density functional theory.: Application to C10H10 and defect migration in crystalline silicon. *Chem. Phys. Lett.* **2001,** *341* (1-2), 185-194.
40. Wales, D. J., *Energy Landscapes*. Cambridge University Press: Cambridge, 2003.
41. Munro, L. J.; Wales, D. J., Defect migration in crystalline silicon. *Physical Review B* **1999,** *59* (6), 3969.
42. Perdew, J. P.; Burke, K.; Ernzerhof, M., Generalized Gradient Approximation Made Simple. *Phys. Rev. Lett.* **1996,** *77* (18), 3865-3868.
43. Tkatchenko, A.; Scheffler, M., Accurate Molecular Van Der Waals Interactions from Ground-State Electron Density and Free-Atom Reference Data. *Phys. Rev. Lett.* **2009,** *102* (7), 073005.
44. Hasnip, P. J.; Refson, K.; Probert, M. I. J.; Yates, J. R.; Clark, S. J.; Pickard, C. J., Density functional theory in the solid state. *Philosophical Transactions of the Royal Society A: Mathematical, Physical and Engineering Sciences* **2014,** *372* (2011).
45. Kresse, G.; Furthmüller, J., Efficiency of ab-initio total energy calculations for metals and semiconductors using a plane-wave basis set. *Computational Materials Science* **1996,** *6* (1), 15-50.
46. Jozefowicz, L. C.; Karge, H. G.; Coker, E. N., Microcalorimetric Investigation of H-ZSM-5 Zeolites Using an Ultrahigh-Vacuum System for Gas Adsorption. *The Journal of Physical Chemistry* **1994,** *98* (33), 8053-8060.
47. Wrabetz, S.; Yang, X.; Tzolova-Müller, G.; Schlögl, R.; Jentoft, F. C., Characterization of catalysts in their active state by adsorption microcalorimetry: Experimental design and application to sulfated zirconia. *J. Catal.* **2010,** *269* (2), 351-358.
48. Sacchi, M.; Wales, D. J.; Jenkins, S. J., Bond-selective energy redistribution in the chemisorption of CH_3D and CD_3H on Pt{1 1 0}-(1 × 2): A first-principles molecular dynamics study. *Computational and Theoretical Chemistry* **2012,** *990* (0), 144-151.
49. Sacchi, M.; Wales, D. J.; Jenkins, S. J., Mode-specificity and transition state-specific energy redistribution in the chemisorption of CH_4 on Ni{100}. *Physical Chemistry Chemical Physics* **2012,** *14* (45), 15879-15887.
50. Sacchi, M.; Wales, D. J.; Jenkins, S. J., Mode-Specific Chemisorption of CH4 on Pt{110}-(1 × 2) Explored by First-Principles Molecular Dynamics. *The Journal of Physical Chemistry C* **2011,** *115* (44), 21832-21842.
51. Bisson, R.; Dang, T. T.; Sacchi, M.; Beck, R. D., Vibrational activation in direct and precursor-mediated chemisorption of SiH_4 on Si(100). *The Journal of Chemical Physics* **2008,** *129* (8), 081103-4.
52. Yoder, B. L.; Bisson, R.; Beck, R. D., Steric Effects in the Chemisorption of Vibrationally Excited Methane on Ni(100). *Science* **2010,** *329* (5991), 553-556.

53. Londero, E.; Karlson, E. K.; Landahl, M.; Ostrovskii, D.; Rydberg, J. D.; Schröder, E., Desorption of n-alkanes from graphene: a van der Waals density functional study. *J. Phys.: Condens. Matter* **2012,** *24* (42), 424212.
54. Hedgeland, H.; Sacchi, M.; Singh, P.; McIntosh, A. J.; Jardine, A. P.; Alexandrowicz, G.; Ward, D. J.; Jenkins, S. J.; Allison, W.; Ellis, J., Mass Transport in Surface Diffusion of van der Waals Bonded Systems: Boosted by Rotations? *The Journal of Physical Chemistry Letters* **2016,** *7* (23), 4819-4824.
55. Calvo-Almazán, I.; Sacchi, M.; Tamtögl, A.; Bahn, E.; Koza, M. M.; Miret-Artés, S.; Fouquet, P., Ballistic Diffusion in Polyaromatic Hydrocarbons on Graphite. *The Journal of Physical Chemistry Letters* **2016,** *7* (24), 5285-5290.
56. Wales, D. J., Energy landscapes: calculating pathways and rates. *Int. Rev. Phys. Chem.* **2006,** *25* (1-2), 237-282.
57. Yang, D.; Yang, N.; Ni, J.; Xiao, J.; Jiang, J.; Liang, Q.; Ren, T.; Chen, X., First-principles approach to design and evaluation of graphene as methane sensors. *Mater. Des.* **2017,** *119*, 397-405.
58. Jiang, Q. G.; Ao, Z. M.; Zheng, W. T.; Li, S., Enhanced hydrogen sensing properties of graphene by introducing a mono-atom-vacancy. *Physical Chemistry Chemical Physics* **2013,** *15* (48), 21016--21022.